The DOI for this manuscript is doi: 10.1175/JPO-D-16-0105.1

Surface relative dispersion in the southwestern Gulf of Mexico

Luis Zavala Sansón*, Paula Pérez-Brunius and Julio Sheinbaum.

CICESE, Carretera Ensenada-Tijuana 3918, 22860 Ensenada, Baja California, Mexico.

* *Corresponding author address:* Luis Zavala Sansón, CICESE, Carretera Ensenada-Tijuana 3918, 22860 Ensenada, Baja California, Mexico.

E-mail: lzavala@cicese.mx

ABSTRACT

Surface dispersion properties in the southwestern Gulf of Mexico are studied by using a set of 441 drifters released during a 7-year period and tracked for 2 months on average. The drifters have a drogue below the surface Ekman layer, so they approximately follow oceanic currents. We follow two different approaches: First, two-particle (or pair) statistics are calculated (relative dispersion and Finite-Scale Lyapunov Exponents, FSLEs). Relative dispersion estimates are consistent with theoretical dispersion regimes of two-dimensional turbulence: an exponential growth during the first 3 days, a Richardson-like regime between 3 and 20 days (in which relative dispersion grows as a power-law in time), and standard dispersion (linear growth) for longer times. The FSLEs yield a power-law regime for scales between 10 and 150 km, but do not detect an exponential regime for short separations (less than 10 km). Robust estimates of diffusivities based on both relative dispersion and FSLEs are provided. Second, two different dispersion scenarios are revealed by drifter trajectories and altimetric data and supported by two-particle statistics: (a) a south-to-north advection of drifters, predominantly along the western shelf of the region, and (b) a retention of drifters during several weeks at the Bay of Campeche, the southernmost part of the Gulf of Mexico. Dominant processes that control the dispersion are the arrival of anticyclonic Loop Current Eddies to the western shelf, and their interaction with the semi-permanent cyclonic structure in the Bay of Campeche.

1. Introduction

The turbulent nature of the oceans and the atmosphere governs the dispersion of physical, chemical and biological tracers in geophysical fluids. In oceanic studies of surface dispersion, floating drifters are often used to calculate the statistical properties of their distribution as they spread. In this article we analyze the dispersion of surface drifters in the Gulf of Mexico (GM), and identify dominant dispersion scenarios associated with the mesoscale circulation. The study is focused on the southwestern part of the GM (hereafter referred to as SGM).

There are important reasons for studying dispersion in the SGM. For instance, large areas over the continental shelf are home to many offshore rigs and oil platforms. It is of interest, therefore, to study the short and long-term fate of pollutants released in the SGM. In particular, it is relevant to determine whether a cloud of tracers will remain in the south or, otherwise, will spread towards northern regions. From a physical point of view, dispersion studies based on the behavior of a large number of drifters are fundamental to elucidate essential features of oceanic turbulence.

Two different approaches are followed. First, two-particle statistics will be discussed in order to investigate the presence of dispersion regimes in the region. Pair statistics are determined by considering the relative dispersion between particles [the mean square pair separation as a function of time, see *e.g.* LaCasce (2008)], and by calculating the so-called finite-scale Lyapunov exponents [FSLEs, the mean separation rate between drifters as a function of their separation, Artale et al. (1997)]. With these computations we aim to get a better understanding on the turbulent dispersion in the region.

Theoretical models describing local and non-local relative dispersion are considered. Non-local dispersion refers to the influence of flow structures larger than the separation between particles (LaCasce 2008), which leads to an exponential growth of the relative dispersion. By contrast,

local dispersion is associated with structures of similar size as the particle separations, and it is characterized by a relative dispersion that grows as a power-law in time. Local and non-local dispersion might be present at different spatial scales, and hence they are useful to identify regimes of turbulent dispersion. For a two-dimensional flow local and non-local dispersion can be related with the slope of the energy spectrum, which is important to parametrize the effect of small scales in numerical models (LaCasce 2010).

Several observational and numerical studies have explored dispersion regimes in other regions [*e.g.* Ollitrault et al. (2005); Haza et al. (2008); Lumpkin and Elipot (2010); Zavala Sansón (2015)] but not yet in the SGM. There are important previous studies in the northern GM. For instance, LaCasce and Ohlmann (2003) investigated both relative dispersion and FSLEs, using drifters with initial separations of $\sim$ 1 km from the SCULP experiment in two regions of the northern shelf of the GM (Ohlmann and Niiler 2005). They found an exponential regime for relative dispersion at early times, associated with non-local dispersion. More recently, Poje et al. (2014) studied the dispersion of a large number of drifters ($\sim$ 300) deployed during the GLAD experiment in the area of the 2010 Deepwater Horizon oil spill. They reported a Richardson-like regime from small scales (less than 1 km) to a few hundred kilometers. Beron-Vera and LaCasce (2016) addressed the dispersion regimes in that same region using a large number of synthetic trajectories from a high-resolution model of the GM. Their results indicate that relative dispersion is initially non-local for small initial separations, and then evolves towards standard dispersion (uncorrelated pair motions) for separations larger than 100 km. We will discuss the presence of local, non-local and standard dispersion in the SGM.

Second, we identify dispersion scenarios determined by the mesoscale circulation in the SGM. We show that the presence and/or interaction of large mesoscale vortices play a key role on drifter dispersion (Olascoaga et al. 2013). One of the main mesoscale circulation features in the SGM

are the well-known anticyclonic Loop Current Eddies (LCEs, with 150 to 300 km in diameter) originally formed at the eastern side of the GM, which usually travel westward until reaching the western margin (Vukovich 2007). Another salient feature is the Campeche gyre (hereafter referred to as CG), a semi-permanent cyclone at the Bay of Campeche (Monreal-Gómez and Salas de León 1997). Based on oceanographic data, Vázquez de la Cerda et al. (2005) documented this feature and concluded that it is seasonally forced by the wind. Using surface drifters and moorings, Pérez-Brunius et al. (2013) found that the CG is generally located in the western Bay of Campeche, probably topographically confined by the southwestern Mexican shelf and the bathymetry at 94°W. Its forcing mechanism is not fully understood yet (Cordero-Quirós 2015). Another important characteristic of the SGM is the presence of intense currents along its western margin that can flow in either direction. On the continental shelf, the direction of the flow depends on the along-coast winds or the presence of eddies interacting with the shelf (Zavala-Hidalgo et al. 2003; Dubranna et al. 2011). Over the continental shelf break, a western boundary current flowing northwards is present throughout the year, driven by the wind stress curl over the northern GM (Sturges 1993; DiMarco et al. 2005). Its intensity varies with the seasonal variability of the wind curl and, at synoptic scales, by the presence of mesoscale eddies (Dubranna et al. 2011).

We find two distinct dispersion scenarios. One of them is dominated by a northward advection of drifters, mainly due to the approach of LCEs to the western shelf and their interaction with the CG. A second scenario involves retention of drifters in the SGM for several weeks.

The paper is organized as follows. In Section 2 the data set is described. Two-particle statistics (relative dispersion and FSLEs) are shown in Section 3, which reflect the dispersion properties over the entire region of study and over several years. In Section 4 we focus on dispersion scenarios associated with mesoscale features. The results are discussed in Section 5.

2. Data

a. Drifters

The set of drifters used in this study is part of a long-term program of oceanographic observations in the GM funded by the Mexican oil industry (PEMEX) and conducted by the Canek Group from CICESE. Being part of a large observational program, the deployment of the drifters was originally designed to study mesoscale circulation features at the southern and central regions of the GM. The large number of launched drifters (see below), allowed us to calculate two-particle statistics, and identify dominant dispersion mechanisms associated with mesoscale vortices.

Several groups of surface drifters were released by aircraft between September 2007 and June 2014, most of them in the SGM. Last records were obtained during August 2014. We use Far Horizon Drifters (FHD, Horizon Marine Inc.), which consist of a cylindrical buoy attached to a parachute that serves as drogue at a nominal depth of 50 m when the buoy drifts in the water [Anderson and Sharma (2008); Sharma et al. (2010)]. In the presence of vertical shear the "para-drogue" may move upwards, as observed in the highly sheared Loop Current (Steve Anderson, Horizon Marine Inc., personal communication). In the SGM, where the vertical shear is expected to be less intense, we estimate that the drogue is likely to stay within 15-20 m of its nominal depth. Mixed layer depths in the GM vary greatly with season, from $\sim$ 20 m in the Summer to over 100 m in Winter [see *e.g.* Zavala-Hidalgo et al. (2014)]. Hence the drifter movement is likely due to mixed-layer flow at least during the cold half of the year. The geographical positions were tracked with a GPS receiver. Additional information on the drifters performance and some pre-processing steps on the data are described by Pérez-Brunius et al. (2013).

A total of 441 drifters were considered, whose initial position lied inside the SGM, as shown in Fig. 1a. The drifters were released by following different strategies. A total of 85 drifters were

launched in different places over the SGM (Fig. 1a, magenta dots), specially at the beginning of the program. The remaining 356 drifters were deployed near five preferential locations selected to sample different regions (Fig. 1a, blue dots). The drifters recorded hourly positions, which were interpolated to regular 3 and 6 h intervals. If a drifter trajectory had an empty record longer than 24 h, then only the initial segment before the information gap is considered. The time of release and the lifetimes of each drifter are presented in Fig. 1b. The average duration of the records is 62 days with a standard deviation of 47 days. The longest lifetime was 218 days.

Figures 1c and d show the initial trajectories from two deployment sites during 30 days, or less for drifters with a shorter lifetime. The first 15-day segments are colored differently than the subsequent sections, which helps to reveal circulation features. Several drifters launched at the western deployment location (panel c) are retained in the SGM, below 22°N, during the first 15 days. This is due to the frequent development of the semi-permanent CG at the Bay of Campeche, which is clearly denoted by many trajectories. When some drifters are able to escape northwards during the following 15 days, they do it preferentially along the western side of the GM. Drifters released at the eastern site (panel d) tend to move northwestward, and most of them are not trapped by the CG. The drifters hardly move towards the central GM, and practically never penetrate into the Yucatan shelf at the eastern side. Rodríguez-Outerelo (2015) discussed some of these observations with the same data set, together with some quantitative estimates: for instance, 32% of the drifters are retained in the Bay of Campeche after 100 days of release, and the residence times are highly variable with a median of 32 days. Work is in progress by one of the authors (PPB) to present these and several other diagnostic measurements with individual drifters. Point source dispersion from the deployment sites is examined in a parallel study (Zavala Sansón et al. 2016).

b. Pairs

Two-particle statistics quantify the separation of two drifters in time and averages over several pairs. As the drifters were released over a period of a few years and in different locations, we perform calculations using the so-called "original" and "chance" pairs (LaCasce and Ohlmann 2003). "Original" pairs correspond to drifters that were deployed simultaneously, while "chance" pairs consist of drifters that approach each other at some time past their release. This is usually done in dispersion studies in order to increase the sampling universe when available data are sparse and difficult to obtain (LaCasce 2008).

The ensembles of drifter pairs for the calculation of relative dispersion and FSLE need to be defined differently. Relative dispersion depends on the initial particle separations (Babiano et al. 1990), hence we considered four pair sets (classes) defined by initial separations between 0-2 km, 4-6 km, 9-11 km, and 29-31 km. The number of pairs in each class as a function of time is shown in Fig. 2a. For the calculation of FSLEs, the pairs are grouped in separation intervals (hereafter, bins) that are 5 km wide and centered at mid-width. The first bin is centered at 2.5 km and the last one at 297.5 km. Fig. 2b shows the number of pairs as a function of the initial separation bins.

3. Two-particle statistics

The evolution of drifter pairs is studied by measuring their relative dispersion (Subsection *a*), and by calculating FSLEs (Subsection *b*). The results identify dispersion regimes at different temporal and spatial scales and quantify diffusivities.

a. Relative dispersion

Relative dispersion refers to the mean-squared separation of particle pairs, and it measures how a cloud of particles spreads in time (LaCasce 2008):

$$\overline{D_i^2}(t,D_0) = \frac{1}{N}\sum_{p\neq q}[x_i^p(t) - x_i^q(t)]^2, \tag{1}$$

where N is the number of pairs initially separated by a given distance D_0, and $x_i^{p,q}$ are the positions of particles p and q, with subindex $i = 1,2$ indicating the zonal and meridional components, respectively. The relative diffusivity is defined as (half) the rate of change of dispersion:

$$Y_i(t,D_0) = \frac{1}{2}\frac{d}{dt}\overline{D_i^2}. \tag{2}$$

The different relative dispersion regimes in geophysical flows depend on the initial separations D_0 with respect to the forcing injection scale D_I. In the ocean, D_I is usually regarded as the scale at which energy is injected to mesoscale eddies by *e.g.* baroclinic instabilities (Babiano et al. 1990), and it is estimated as the internal Rossby radius of deformation. Here we measure $\overline{D_i^2}$ directly from drifter data and then compare with theoretical dispersion regimes expected for two-dimensional turbulence (presented in the Appendix).

Figure 3 shows plots of relative dispersion components calculated from (1), using sets of pairs with different initial separations. Both components grow at a similar rate, showing that dispersion is isotropic during 15-20 days, approximately. After 20 days the growth of zonal dispersion is diminished, presumably due to the presence of the western boundary of the GM, while the meridional component continues growing for a longer period. The fitted curves suggest three different regimes: (1) an exponential growth from 0 to 3 days, (2) a power-law from 3 to 18 days, (3) a linear growth in time after 20 days which indicates standard dispersion (more evident for the meridional component). These dispersion regimes are further explored below. The curves are calculated by using 91, 138, 163, and 377 pairs at day 0 for each separation class, respectively. These numbers

decreased to 55, 78, 98, and 232 pairs at day 20, respectively (Fig. 2a). The fitting coefficients and the corresponding errors are determined by least squares. The errors are very small (less than 10%). However, the error size is sensitive to the time interval chosen to make the fit, *i.e.* by increasing or reducing the number of data in the fitting interval, the exponents might vary another 5-10%.

The relative dispersion alone is not conclusive to determine dispersion regimes, as discussed by LaCasce (2010) [see also Koszalka et al. (2009), Lumpkin and Elipot (2010)], mainly because at early times it might be possible to fit either a power-law in time or an exponential growth. A method used to distinguish dispersion regimes are the Probability Density Functions (PDFs) of pair separations. In the context of a two-dimensional, isotropic turbulent flow, analytical PDFs of the exponential and Richardson regimes have been calculated in previous studies, as shown in the Appendix. The aim here is to analyze whether or not such theoretical profiles represent the measured PDFs and the corresponding moments. Since dispersion is nearly isotropic up to about 20 days, we will use the total dispersion $\overline{D^2}$.

Figure 4 shows examples of the PDFs at fixed times t_a, re-scaled with the corresponding standard deviation of the separations [Jullien et al. (1999); Scatamacchia et al. (2012)]. Superposed to the PDF bars are the theoretical curves for the exponential (gray) and Richardson (dashed) regimes, given by expressions (A3) and (A7), respectively. Given both the relative dispersion at the chosen time, $\overline{D^2}(t_a)$, and the initial separation, D_0, the free parameters T and β are obtained from the expressions for relative dispersion (A4) and (A8). For the exponential model $T = 8t_a/\log[\overline{D^2}(t_a)/D_0^2]$, while β is calculated numerically for the Richardson model. Values for each example are shown in the figure caption.

In order to determine whether the theoretical distributions are similar to the observed PDFs as they evolve in time, we apply the Kolmogorov-Smirnov test (Beron-Vera and LaCasce 2016). The

result of the test is positive (the theoretical and the empirical distributions are not significantly different) when the Kolmogorov-Smirnov probability p is larger than 0.05 (the significance level). The results from 1 to 10 days are shown in the insets of Fig. 4 for each separation class. When the KS test is positive, T and β can be calculated at each time as explained above, and then representative values of the parameters are obtained by averaging the results.

The KS tests for short separations (Figs. 4a and b) indicate that the exponential model represents well the observed PDFs between 1 and 4 days, approximately, while the Richardson model is not similar to the observed data, except for a single case in panel b. The average time scale in the exponential model is $T = 5.21 \pm 1.01$ d and $T = 7.44 \pm 0.96$ for 1 and 5 km separations, which implies a growth rate $8/T$ between 1.5 and 1 d^{-1}, respectively. These values compare well with the growth rates obtained by fitting exponential curves to relative dispersion during the first three days (Figs. 3a and b). This supports the hypothesis of non-local dispersion for short initial separations. For larger separations (Figs. 4c and d) the Richardson curves represent better the measured PDFs than the exponential model, according to the KS tests. This behavior is consistent with local dispersion at larger initial separations, as curves in Figs. 3c and d suggested. The average β-parameter in panel c (10 km initial separations) is $\beta = 0.93 \pm 0.08$ $km^{2/3}$ d^{-1}, and in panel d (30 km) $\beta = 0.91 \pm 0.02$ $km^{2/3}$ d^{-1}.

Using the T and β-values, the theoretical curves of relative dispersion, equations (A4) and (A8) in the Appendix, are calculated. Fig. 5 shows a comparison with the curves computed with data, using the same initial separations as before. As a reference, the asymptotic curve t^3 of the Richardson regime is included, as well as the linear dispersion curve t for long times. The data are well fit by both the exponential and the Richardson curves during the first days for all initial separations, as shown in the PDFs analysis. At intermediate times (up to 15-20 days) the

Richardson curve represents much better all cases. For longer times, dispersion grows as t as in the standard dispersion regime.

We also considered the time-dependent normalized fourth moment of the particle separations or kurtosis K (see Appendix). The kurtosis measures the relative weight of the tails of a distribution, and its time evolution provides information about the PDF similarity. Figure 6 presents the kurtosis estimated from data for the four sets of pairs with different initial separations. The theoretical curve for the exponential regime (A5) is also included, as well as the asymptotic value of the Richardson ($K = 5.6$) and standard dispersion ($K = 2$) regimes. The kurtosis for the shortest separation (0-2 km, Fig. 6a) rapidly grows to high values (more than 20), approximately following the exponential growth of the theoretical curve. This result agrees with the analysis of the PDFs and supports the hypothesis of non-local dispersion. This statement cannot be conclusive, however, because the errors are significant for higher order statistics. Koszalka et al. (2009) found a very similar behavior of the kurtosis in time and a corresponding large error using data from the Nordic Seas. For larger initial separations (4-5 and 9-11 km, Figs. 6b and c), the kurtosis approaches the asymptotic value of the Richardson regime at intermediate times. For later times, the kurtosis in all cases tends to the asymptotic limit of standard dispersion.

Relative diffusivity Y is calculated as (half) the time derivative of the relative dispersion curve. Figure 7 shows the diffusivities in terms of the separation scale, as well as those derived from the theoretical models. The curves tend to follow the 4/3 Richardson's law (A6), a behavior that is further examined with the FSLEs in next subsection.

b. Finite-Scale Lyapunov Exponents

A different approach to study particle pairs is to use distance as the independent variable, which leads to the FSLEs (Artale et al. 1997). For this measure, two particles initially separated a dis-

tance δ are considered; then the time τ at which the two drifters separate a given distance $\alpha\delta$ is calculated, with $\alpha > 0$ (here we use $\alpha = \sqrt{2}$). The calculation is repeated for all available pairs. The FSLEs are defined as

$$\lambda(\delta) = \frac{1}{< \tau(\delta) >} \log \alpha, \tag{3}$$

where $< \tau(\delta) >$ is the average of all the separation times for a given δ. The quantity $\lambda(\delta)$ is the rate of divergence between two particle positions, as the conventional Lyapunov exponent, but now calculated with finite separations (d'Ovidio et al. 2004). A diffusivity scale can be simply calculated as $\delta^2\lambda$.

The relation λ vs. δ defines different dispersion regimes in terms of the size of the energy containing eddies D_I. In a range of very short scales, $\delta << D_I$, the FSLEs are constant. An intermediate Richardson regime corresponds to the size of the energy containing eddies, which implies a relation $\lambda(\delta) \propto \delta^{-2/3}$. For larger separations $\delta >> D_I$, particle velocities are uncorrelated and standard diffusion takes place, which corresponds with $\lambda(\delta) \propto \delta^{-2}$ (Artale et al. 1997; Lacorata et al. 2001).

Figure 8a shows the FSLEs using drifter data with temporal resolutions of 6 and 3 h. In both cases the curves are almost indistinguishable. For small δ, the exponential regime characterized by constant λ is not observed. A possible reason is the bin size, 5 km, which is comparable to the scale range expected for this regime (as inferred from the relative dispersion plots for short separations). Smaller bins were calculated but they contain very few pairs, making the statistics unreliable. For larger distances, an intermediate dispersion regime is identified by fitting a straight line between 12.5 and 147.5 km. This closely corresponds with the Richardson regime, for which the slope is $-2/3$. For larger distances (between 150 and 300 km), the curves do not become steeper, and therefore the standard diffusion regime (slope -2) is not observed. Thus, the FSLEs detect only an intermediate Richardson-like dispersion regime.

The diffusivity scale $\delta^2\lambda$ is calculated for the 6h resolution data, and plotted in Fig. 8b as a function of δ. A power-law is fitted over the intermediate range found above. The exponent is 1.39 ± 0.03, so the curve closely resembles the 4/3 Richardson's law. In the range of interest, the FSLE diffusivities are consistent with the relative diffusivities Y shown in Fig. 7. In order to show this, both quantities are superposed in Fig. 8b. Relative diffusivities are multiplied by 1/3, and hence the relationship between them is $\delta^2\lambda \sim Y/3$. The number of available pairs in previous results is about 120 for the smallest bin $\delta \sim 2.5$ km, and rapidly grows to more than 1500 for $\delta \sim 180$ km (Fig. 2b).

4. Dispersion scenarios in the SGM

To draw the dispersion scenarios we first identify the periods in which the presence of mesoscale vortices affect the distribution of drifters (Subsection *a*), and then we examine the statistical properties of dispersion at these times (Subsection *b*).

a. Dominant mesoscale features

In terms of dispersion, the most relevant mesoscale *features* in the SGM are the anticyclonic vortices shed by the Loop Current at the eastern GM (defined as LCEs in the Introduction), and the semi-permanent cyclonic structure at the Bay of Campeche (defined as CG), located at the southernmost region of the GM. The most important *processes* in which these structures are involved are: (i) the passage of the LCEs through the region as they drift westward, (ii) their collision with the western shelf, and (iii) the development of the CG and its interactions with the LCEs.

The occurrence and evolution of these processes are examined during the whole period of study (84 months). The procedure consisted of superposing all available drifter trajectories for each

month, together with the satellite altimetry map at day 15 of the corresponding month. From this analysis two dispersion scenarios are identified:

(1) An intense south-to-north advection of drifters, which takes place predominantly along the western shelf of the GM. It is mostly related with the interaction of LCEs with the CG located in the southernmost region. During this process, anticyclones capture drifters in the periphery of the CG and strongly pushes them northward along the western boundary of the SGM. Some other features that might play a role are western boundary currents and smaller vortices along the shelf.

(2) A retention or blocking of drifters at the Bay of Campeche during several weeks. This scenario occurs when the CG is well-formed and confined to southern latitudes, where drifters are retained.

The northward advection scenario is observed in 26 months, the blocking scenario takes place in 26 different months, and during 32 months neither of the two scenarios is clearly present. The northward advection scenario is identified when 25% of drifters in a given month move beyond 24°N. The blocking scenario is determined when 75% of the drifters remain south from 22°N. The scenarios may occur at any time of the year, because the mesoscale circulations like the LCEs or the CG are not significantly associated with any season.

The northward advection and the blocking of drifters might be linked. Figure 9 presents a sequence of six consecutive months that illustrate the alternate occurrence of both scenarios. In November 2011 the CG is clearly formed at 20°N, 95°W; as a consequence, there is an almost complete retention of drifters in the south. Meanwhile, an irregular LCE is arriving from the east at 24°N. In December 2011 the CG has a well-defined elliptical shape, oriented in NW-SE direction, apparently due to the approach of the LCE at 23°N, 93°W. In January 2012, the interaction between

the LCE and the CG is evident from the strong deformations in both structures. During this month, the intense northward advection scenario is verified, as the drifter trajectories clearly indicate. In February 2012 the anticyclone continues approaching the shelf, and starts blocking the northward passage of drifters. The CG is strongly deformed and further confined to southern latitudes in March 2012, so the blocking scenario is verified again. The collision of the anticyclone with the shelf continues in April 2012. During this process the vortex is notably damped and displaced northward, allowing the passage of drifters to the north again.

b. Relative dispersion and FSLEs

Here we calculate pair statistics for the dispersion scenarios, in order to illustrate quantitative differences between them. Relative dispersion components during the northward advection and blocking events are presented in Figs. 10a and b, respectively, for mean initial separations of 30 km. The curves are calculated with (1), but now using only the available pairs in the corresponding periods of 26 months. There are nearly 150 pairs at early times and about 80 pairs after 20 days. In both cases the dispersion is isotropic up to 5 days, approximately. After this time, the northward advection scenario (panel a) becomes anisotropic, with the meridional component growing faster than the zonal component. Power-laws in time are fitted to both components between 3 and 20 days, in which the exponent clearly differs between the zonal and the meridional components. In contrast, during the blocking scenario (panel b) relative dispersion remains isotropic up to 20 days, indicating that there is no preferred direction during the spread of drifters retained in the SGM.

The FSLEs are calculated for the dispersion scenarios. The λ vs. δ curves are shown in Fig. 11a. Analogous to the general case, the exponential regime (constant λ at small δ) is not observed. For intermediate separations (between 47.5 and 122.5 km), a Richardson-like regime is found in both scenarios, with a slope somewhat smaller than -2/3 (0.56 ± 0.07). However, at about $\delta \sim 125$ km

the curves clearly diverge: the northward advection case approximately follows the same trend, while the blocking scenario decays faster. The associated slope between 127.5 and 297.5 km is -1.23 ± 0.05, indicating a slower dispersion than for shorter separations, but not as steep as -2 as in standard diffusion. Diffusivities in terms of δ are calculated and plotted in Fig. 11b. The divergence of the curves for the two dominant scenarios is captured again. Note that the scale-dependent diffusivities approximately follow the 4/3 Richardson's law in the first range, while the diffusivity in the blocking case is sensibly decreased in the second range. The number of pairs within the δ-ranges in which the power-laws are fitted is more than 200.

5. Discussion and conclusions

In Section 3 we calculated two-particle statistics for a large set of drifters in the SGM, and in Section 4 two particular dispersion scenarios were identified, which were clearly linked with the mesoscale circulation. We will now discuss the results separately.

a. Dispersion properties in the SGM

Relative dispersion, PDFs of separations and kurtosis as function of time support the presence of an exponential regime at early times for short initial separations (0-2 km). This assertion is based on the fact that the time-dependent statistics show a similar trend as the theoretical PDFs and their moments, despite the associated errors, as shown *e.g.* in Figs. 3a to 6a. The e-folding time is between 0.5 and 1 day. Similar analyses were performed both for the SCULP and GLAD data sets in the northern GM by LaCasce (2010) and Beron-Vera and LaCasce (2016), respectively. In both cases the authors concluded that dispersion is non-local in that region, with an e-folding time of ~ 1 day. In the Nordic Seas, Koszalka et al. (2009) found an e-folding time of roughly 0.5 days.

For larger separations we find an exponential growth of relative dispersion (for instance, in Figs. 3c and 3d). However, this does not imply an exponential regime because the PDFs and the corresponding kurtosis do not behave as in this model, as shown in Figs. 4c-d and 5c-d. An important conclusion is that an exponential growth in relative dispersion does not necessarily imply the presence of non-local dispersion (LaCasce, 2010). The power-law regime of relative dispersion found at later times (between 3 and 20 days) can be regarded as a Richardson-like regime, a result that is supported by the PDFs and their moments.

The FSLEs also detect a Richardson-like regime for scales between 10 and 150 km, approximately (Fig. 8a). However, the FSLEs fail to detect both the exponential regime for short separations and the standard dispersion regime for larger scales. Some possible explanations for this might be related to the inherent limitations of the FSLEs (Karrasch and Haller 2013). Another reason might be the influence of inertial motions, which affect scale-dependent statistics like the FSLEs, while keeping time-dependent metrics (PDFs and statistical moments) unaffected (Beron-Vera and LaCasce 2016). Also, for small separation ranges the FSLE calculations can be sensitive to data temporal resolution (Lumpkin and Elipot 2010). Therefore, in terms of general dispersion properties, the FSLEs are mainly used to determine the Richardson-like range and to estimate the scale-dependent diffusivities ($\delta^2\lambda$) according with the 4/3 Richardson's law. When comparing with relative diffusivities, it is found that $Y \sim 3\delta^2\lambda$ (Fig. 8b).

Care should be taken when interpreting the possible presence of a Richardson regime. Super-diffusive regimes with a power-law behavior t^γ ($\gamma > 1$) have been reported in some other studies. For example, LaCasce and Ohlmann (2003) reported $\gamma \sim 2.2$ in the northern continental shelf of the GM; Haza et al. (2008) found $\gamma \sim 1.9$ in the Adriatic Sea; Zavala Sansón (2015) measured $\gamma \sim 1.7$ along the Gulf of California. This behavior is attributed to shear dispersion by some of

these authors. Here we observed that most of the drifters tend to escape over the western shelf of the GM, where strong shear is probably present.

Beron-Vera and LaCasce (2016) pointed out the importance of the number of independent samples in the drifter data set. By means of high-resolution numerical experiments, these authors showed that releasing particles at very close initial positions ($\sim$ 1 km) in a very compact area leads to having very few independent pairs, which in turn obscures the exponential regime in favor of the Richardson regime. Their simulations mimicked the drifters in the GLAD experiment conducted in the northern GM (Poje et al. 2014). Based on these results, Beron-Vera and LaCasce (2016) recommend to measure two-particle statistics with sets of pairs distributed over a wide range of scales, in order to get a large number of independent samples able to detect both local and non-local dispersion. In the present study we use a large set of drifters (441), most of them released at very different locations and at different times during a 7-year period, *i.e.* most of them were not simultaneously released. As a result, most of realizations can be considered independent.

b. Dispersion scenarios

Another fundamental result is that the surface Lagrangian dispersion is strongly influenced by mesoscale circulations related with some characteristic vortical structures at the SGM. The most important mesoscale processes consist of the approach of anticyclonic LCEs to the western shelf, the eventual collision with the topography, and the interaction with the CG. From these processes, two main dispersion scenarios emerged. One of them consists of the northward advection of drifters, mostly related with the interaction of LCEs with the CG located in the southernmost region. The other scenario is the blocking of drifters in the SGM associated with the size, strength, and frequent formation of the CG, which acts as a retention feature. In some cases the presence of

a LCE that has approached the western shelf might inhibit the northward motion of drifters, and contribute to the retention at the south.

There are a number of additional situations that might generate advection or retention of drifters from the SGM, such as the generation and/or merging of smaller cyclones and anticyclones in the region. There is also the presence of the western boundary current associated with the wind stress curl over the northern GM (Sturges 1993; DiMarco et al. 2005), that might be responsible for the northward advection of drifters, particularly in Summer when it is strongest. Nevertheless, most of exchange of drifters with the northern GM seems to be driven by the interaction of the CG with LCEs.

Two-particle statistics were calculated in order to distinguish both scenarios quantitatively. It was verified that relative dispersion is anisotropic during the northward advection scenario: the meridional component grows faster than the zonal component. By contrast, relative dispersion is isotropic during the blocking events. The FSLEs showed an intermediate Richardson-like regime, between 50 and 120 km, for both scenarios. At about 125 km the FSLE curves diverge abruptly: the northward advection curve maintains the same tendency, while the blocking curve drops.

The results might have important implications for dispersion problems in the SGM because of the retentive nature of the CG. Consider, for instance, the release of a patch of tracers somewhere in the region, and the consequent necessity to know their evolution. By examining altimetry maps or the output of operational numerical simulations, the presence of LCEs and the development of the CG could be determined. Then, depending on the position, size and strength of these structures, it might be possible to infer the occurrence of one of the dispersion scenarios, or even the consecutive occurrence of both of them, as in the example shown in Fig. 9. The prediction might fail in several cases; for instance, when the LCEs or the CG are not present or clearly defined, or when there are additional structures or complicated patterns not considered here. Nevertheless, knowing the

essential role of the dominant mesoscale features provides a useful tool to forecast the evolution of floating objects or substances in the SGM.

It has been shown that the continuous release of drifters during several years in the region shed important light on their fate due to the surface circulation. With this information we have been able to calculate not only general dispersion properties, but to depict some basic scenarios that provide a practical tool for understanding dispersion mechanisms, and to help on the prediction of future tracer trajectories. However, the present results are still a rough estimation of dominant dispersion events. In order to improve such estimations, more detailed studies (using large sets of drifters and suitable deployment strategies) are required.

Acknowledgments. Drifter data funded by PEMEX Exploración y Producción under CICESE-PEMEX contracts SAP nos. 428217896, 428218855, and 428229851. This is a contribution of the Gulf of Mexico Research Consortium (CIGoM), supported by the National Council of Science and Technology of Mexico - Secretariat of Energy-Hydrocarbons Trust, project 201441.

APPENDIX

Turbulent dispersion regimes

Consider a set of particles in a homogeneous, isotropic, two-dimensional, turbulent flow. The original theory of Richardson (1926) assumes that, as the particles spread, the Probability Density Function (PDF) of relative separations D obeys a Fokker-Planck equation

$$\frac{\partial P}{\partial t} = \frac{1}{D}\frac{\partial}{\partial D}\left(DY\frac{\partial P}{\partial D}\right), \tag{A1}$$

where P is the PDF, and Y is the relative diffusivity, which in general depends on D. Solutions of this equation for different forms of $Y(D)$ are presented in detail by LaCasce (2010) and Graff et al.

(2015) [see also Beron-Vera and LaCasce (2016)]. Here we summarize some relevant results for our own purposes.

At time $t = 0$ an initial delta-function distribution $P(D,0) = (2\pi D)^{-1}\delta(D - D_0)$ is assumed, where D_0 is the initial separation. This form implies that the probability is normalized, *i.e.* $2\pi\int_0^\infty PDdD = 1$. The separation moments derived from the PDFs are $\overline{D^n}(t) = 2\pi\int_0^\infty D^{n+1}PdD$, from which relative dispersion $\overline{D^2}$, the second moment, is calculated with $n = 2$. The normalized fourth moment ($n = 4$) is the kurtosis, $K = \overline{D^4}/(\overline{D^2})^2$.

Let D_I be the energy injection scale. When $D_0 < D_I$ the particles separate exponentially under the influence of structures larger than the initial separation distance (non-local dispersion). This is the enstrophy cascade regime in two-dimensional turbulence (Lin 1972), in which the diffusivity is proportional to the relative dispersion

$$Y = \chi^{1/3}D^2, \tag{A2}$$

being the enstrophy transferred at a rate χ to length scales shorter than D_I. Expression (A2) implies an exponential growth of relative dispersion with a timescale $T \propto \chi^{-1/3}$. The PDF is given by

$$P(D,t) = \frac{1}{4\pi^{3/2}D_0^2(t/T)^{1/2}}\exp\left[-\frac{(\ln D/D_0 + 2t/T)^2}{4t/T}\right], \tag{A3}$$

and the relative dispersion is

$$\overline{D^2} = D_0^2\exp\left(8\frac{t}{T}\right). \tag{A4}$$

The kurtosis grows exponentially at the same rate as the relative dispersion

$$K = \exp\left(8\frac{t}{T}\right), \tag{A5}$$

indicating that the PDF is not self-similar: its peak becomes shaper and the tails are increasingly extended. This regime is usually referred to as exponential, Kraichnan-Lin law (Babiano et al. 1990), or Lundgren regime (LaCasce 2010).

For initial separations $D_0 \geq D_I$, the (inverse) energy cascade regime is verified, in which the diffusivity is assumed as

$$Y = \varepsilon^{1/3} D^{4/3}, \tag{A6}$$

which is known as the 4/3 Richardson's law, with ε the rate of energy transfer. This is called the Richardson regime, for which the PDF solution is

$$P(D,t) = \frac{1}{(4/3)\pi\beta(D_0 D)^{2/3} t} I_2 \left[\frac{9(D_0 D)^{1/3}}{2\beta t} \right] \exp\left[-\frac{9(D_0^{2/3} + D^{2/3})}{4\beta t} \right], \tag{A7}$$

where I_2 is the second-order Bessel function and $\beta \propto \varepsilon^{1/3}$. An explicit expression for the relative dispersion was derived by Graff et al. (2015)

$$\overline{D^2} = \frac{5!}{2} \left(\frac{4\beta t}{9} \right)^3 \exp\left[-\frac{9D_0^{2/3}}{4\beta t} \right] M\left(6, 3, \frac{9D_0^{2/3}}{4\beta t} \right), \tag{A8}$$

with M the Kummer's function. The asymptotic limit for long times is $\overline{D^2} \approx 5.2675\beta^3 t^3$, which expresses the well-known t^3 behaviour of relative dispersion within the Richardson regime. The kurtosis varies from $K = 1$ at $t = 0$ to the asymptotic value $K = 5.6$ for later times, so the PDF becomes self-similar.

For $D_0 >> D_I$ particles are sufficiently far from each other, at a much larger scale than the energy containing eddies. Thus, they disperse randomly and the diffusivity is approximately constant $Y \propto constant$. This is the standard diffusion regime. The relative dispersion is proportional to time $\overline{D^2} = 2Yt$ and the kurtosis is $K = 2$ (the PDF is self-similar).

References

Anderson, S. P., and N. Sharma, 2008: Satellite-tracked drifter measurements of inertial currents in the Gulf of Mexico. *Proceedings of the 2008 IEEE/OES 9th Working Conference on Current Measurement Technology*, Charleston, SC, IEEE/OES, 285-288, [doi: 10.1109/CCM.2008.4480882].

Artale, V., G. Boffetta, A. Celani, M. Cencini, and A. Vulpiani, 1997: Dispersion of passive tracers in closed basins: Beyond the diffusion coefficient. *Phys. Fluids*, **9**, 3162–3171.

Babiano, A., C. Basdevant, P. LeRoy, and R. Sadourny, 1990: Relative dispersion in two-dimensional turbulence. *J. Fluid Mech*, **214**, 535–557.

Beron-Vera, F. J., and J. H. . LaCasce, 2016: Statistics of simulated and observed pair separations in the Gulf of Mexico. *J. Phys. Oc.*, **46**, 2183–2199.

Cordero-Quirós, N., 2015: Variabilidad estacional de la circulación inducida por viento en el Golfo de Campeche (in Spanish). MSc thesis, CICESE, 39 p. *[Available from CICESE library www.cicese.edu.mx]*.

DiMarco, S. F., D. Worth, D. N. Jr., and R. O. Reid, 2005: A statistical description of the velocity fields from upper ocean drifters in the Gulf of Mexico. *Circulation in the Gulf of Mexico: Observations and Models*, W. Sturges, and A. Lugo-Fernandez, Eds., Geophysical Monograph Series, Vol. 161, American Geophysical Union, 101–110.

d'Ovidio, F., C. López, E. Hernández-García, and V. Fernández, 2004: Mixing structures in the Mediterranean sea from Finite-Size Lyapunov Exponents. *Geophys. Res. Lett.*, **31**, L17 203.

Dubranna, J., P. Pérez-Brunius, M. López, and J. Candela, 2011: Circulation over the continental shelf of the western and southwestern Gulf of Mexico. *J. Geophys. Res.*, **116**, C08 009.

Graff, L. S., S. Guttu, and J. H. LaCasce, 2015: Relative dispersion in the atmosphere from reanalysis winds. *J. Atmos. Sci.*, **72**, 2769–2785.

Haza, A. C., A. C. Poje, T. M. Ozgokmen, and P. Martin, 2008: Relative dispersion from a high-resolution coastal model of the Adriatic Sea. *Ocean Modell.*, **22**, 48–65.

Jullien, M. C., J. Paret, and P. Tabeling, 1999: Richardson pair dispersion in two-dimensional turbulence. *Phys. Rev. Lett.*, **82**, 2872–2875.

Karrasch, D., and G. Haller, 2013: Do Finite-Size Lyapunov Exponents detect coherent structures? *Chaos*, **23**, 043 126.

Koszalka, I., J. H. LaCasce, and K. A. Orvik, 2009: Relative dispersion in the Nordic Seas. *J. Mar. Res.*, **67**, 411–433.

LaCasce, J. H., 2008: Lagrangian statistics from oceanic and atmospheric observations. *Lect. Notes Phys.*, **744**, 165–218.

LaCasce, J. H., 2010: Relative displacement probability distribution functions from balloons and drifters. *J. Mar. Res.*, **68**, 433–457.

LaCasce, J. H., and C. Ohlmann, 2003: Relative dispersion at the surface of the Gulf of Mexico. *J. Mar. Res.*, **61**, 285–312.

Lacorata, G., E. Aureli, and A. Vulpiani, 2001: Drifter dispersion in the Adriatic Sea: Lagrangian data and chaotic model. *Ann. Geophys.*, **19**, 121–129.

Lin, J. T., 1972: Relative dispersion in the enstrophy-cascading inertial range of homogeneous two-dimensional turbulence. *J. Atmos. Sci.*, **29**, 394–396.

Lumpkin, R., and S. Elipot, 2010: Surface drifter pair spreading in the North Atlantic. *J. Geophys. Res. Oceans*, **115**, C12 017.

Monreal-Gómez, M. A., and D. Salas de León, 1997: Circulación y estructura termohalina del Golfo de México. *Contribución a la Oceanografía Física en México*, M. Lavín, Ed., Monografía de la Unión Geofísica Mexicana, Vol. 3, Unión Geofísica Mexicana, 183–199.

Ohlmann, J. C., and P. P. Niiler, 2005: Circulation over the continental shelf in the northern Gulf of Mexico. *Progr. Oceanogr.*, **64**, 45–81.

Olascoaga, M. J., and 13 coauthors, 2013: Drifter motion in the Gulf of Mexico constrained by altimetric Lagrangian coherent structures. *Geophys. Res. Lett.*, **40**, 6171–6175.

Ollitrault, M., C. Gabillet, and A. C. de Verdiere, 2005: Open ocean regimes of relative dispersion. *J. Fluid Mech.*, **533**, 381–407.

Pérez-Brunius, P., P. García-Carrillo, J. Dubranna, J. Sheinbaum, and J. Candela, 2013: Direct observations of the upper layer circulation in the southern Gulf of Mexico. *Deep Sea Res. Part II: Topical Studies in Oceanography*, **85**, 182–194.

Poje, A. C., and 18 coauthors, 2014: The nature of surface dispersion near the Deepwater Horizon oil spill. *Proc. Nat. Acad. Sci. USA*, **111**, 12,693–12,698.

Richardson, L. F., 1926: Atmospheric diffusion on a distance-neighbor graph. *Proc. Roy. Soc. A*, **110**, 709–737.

Rodríguez-Outerelo, J., 2015: Conectividad del Golfo de Campeche con el resto del Golfo de México a partir de datos lagrangianos reales y simulados (in Spanish). MSc thesis, CICESE, 58 p. *[Available from CICESE library www.cicese.edu.mx].*

Scatamacchia, R., L. Biferale, and F. Toschi, 2012: Extreme events in the dispersions of two neighboring particles under the influence of fluid turbulence. *Phys. Rev. Lett.*, **109**, 144 501–5.

Sharma, N., P. Brickley, G. Owen, and P. Coholan, 2010: Use of air-deployed drogued drifting buoys for oil spill tracking. *Proceedings of OCEANS 2010 MTS/IEEE*, Seattle, WA, MTS/IEEE, 1-9, [doi: 10.1109/OCEANS.2010.5663921].

554 Sturges, W., 1993: The annual cycle of the western boundary current in the Gulf of Mexico. *J.*
555 *Geophys. Res.*, **98**, 18,053–18,068.

556 Vázquez de la Cerda, A., R. O. Reid, S. F. DiMarco, and A. E. Jochens, 2005: BOC circulation: an
557 update. *Circulation in the Gulf of Mexico: observations and models*, W. Sturges, and A. Lugo-
558 Fernandez, Eds., Geophysical Monograph Series, Vol. 161, American Geophysical Union, 279–
559 293.

560 Vukovich, F. M., 2007: Climatology of ocean features in the Gulf of Mexico using satellite remote
561 sensing data. *J. Phys. Oc.*, **37**, 689–707.

562 Zavala-Hidalgo, J., R. Romero-Centeno, A. Mateos-Jasso, L. S. Morey, and B. Martinez-Lopez,
563 2014: The response of the Gulf of Mexico to wind and heat flux forcing: What has been learned
564 in recent years? *Atmósfera*, **27**, 317–334.

565 Zavala-Hidalgo, J. S., L. S. Morey, and J. J. OBrien, 2003: Seasonal circulation on the western
566 shelf of the Gulf of Mexico using a high-resolution numerical model. *J. Geophys. Res.*, **108**,
567 C123 389.

568 Zavala Sansón, L., 2015: Surface dispersion in the Gulf of California. *Progr. Oceanogr.*, **137**,
569 24–37.

570 Zavala Sansón, L., P. Pérez-Brunius, and J. Sheinbaum, 2016: Point source dispersion of surface
571 drifters in the southern Gulf of Mexico. *Submitted to Environ. Res. Lett.*

LIST OF FIGURES

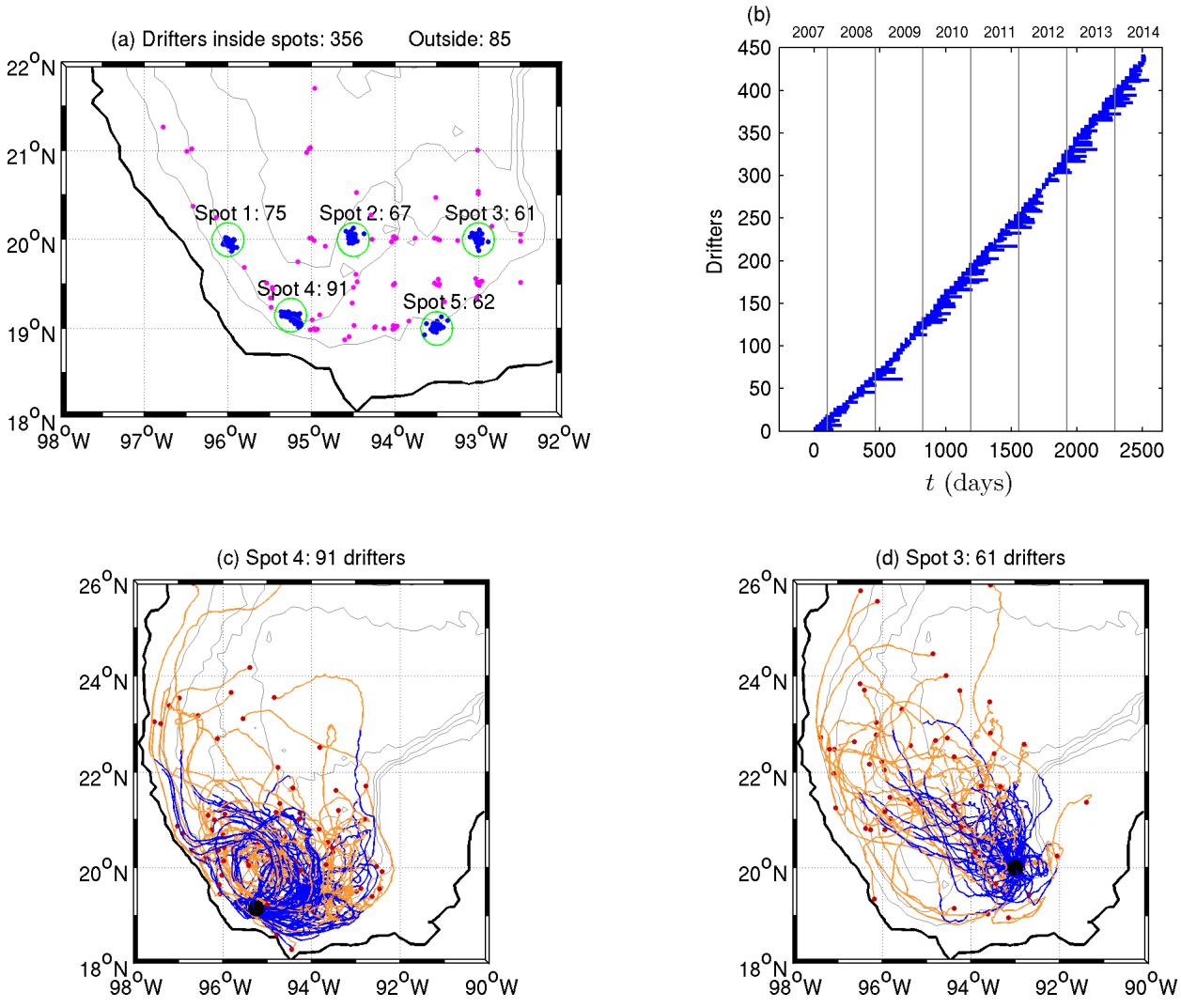

FIG. 1. (a) Initial positions of 441 drifters deployed in the SGM. Blue dots indicate the initial positions of 356 drifters released in five preferential locations marked with a circle (20 km radius) centered at: 20°N, 96°W (spot 1), 20°N, 94.5°W (spot 2), 20°N, 93°W (spot 3), 19.15°N, 95.25°W (spot 4), and 19°N, 93.5°W (spot 5). Numbers aside the circles indicate the amount of deployments. Magenta dots point out the initial positions of 85 drifters released outside the spots. Topography contours (500, 1500, 2500 and 3500 m) are denoted with thin black lines. (b) Time of release and lifetime of the 441 drifters. (c) Trajectories of drifters released at spot 4 (indicated with a big black dot). The maximum duration of the trajectories is 30 days. The first 15 days are colored in blue; subsequent days are colored in orange. Red dots indicate the final position. (d) Same as panel c for drifters released at spot 3.

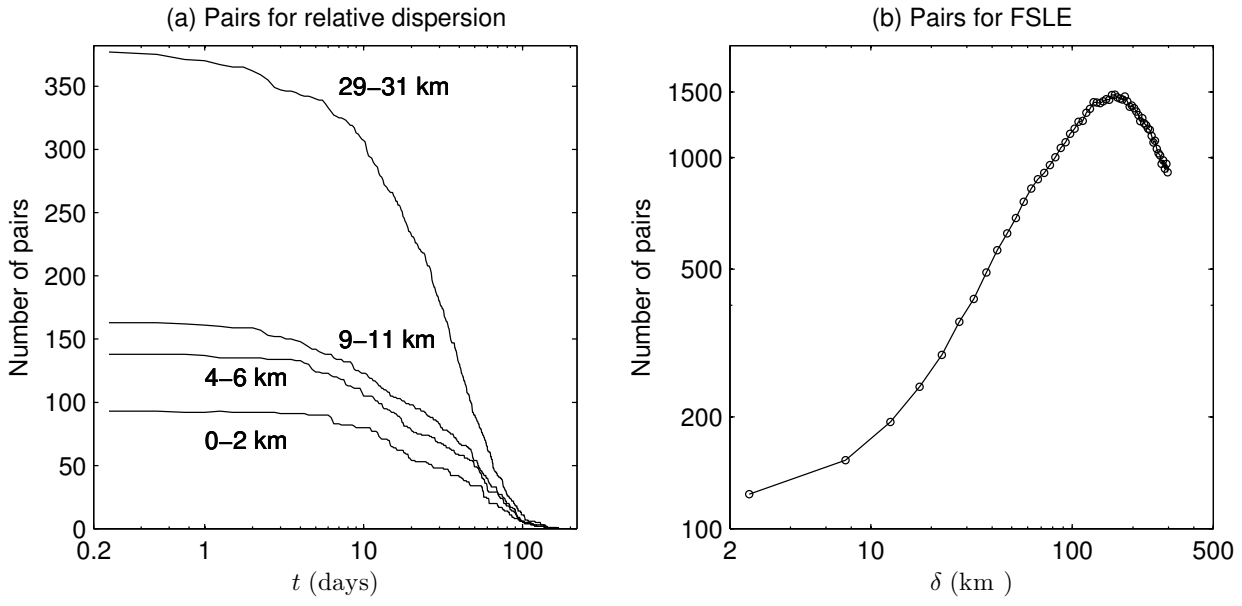

660 FIG. 2. (a) Number of pairs as a function of time for sets defined by different initial separations (used for
661 measuring relative dispersion). (b) Number of pairs as a function of distance bins δ (used for measuring FSLEs).
662 The bins are 5 km wide; the first (last) bin is centered at 2.5 km (297.5 km).

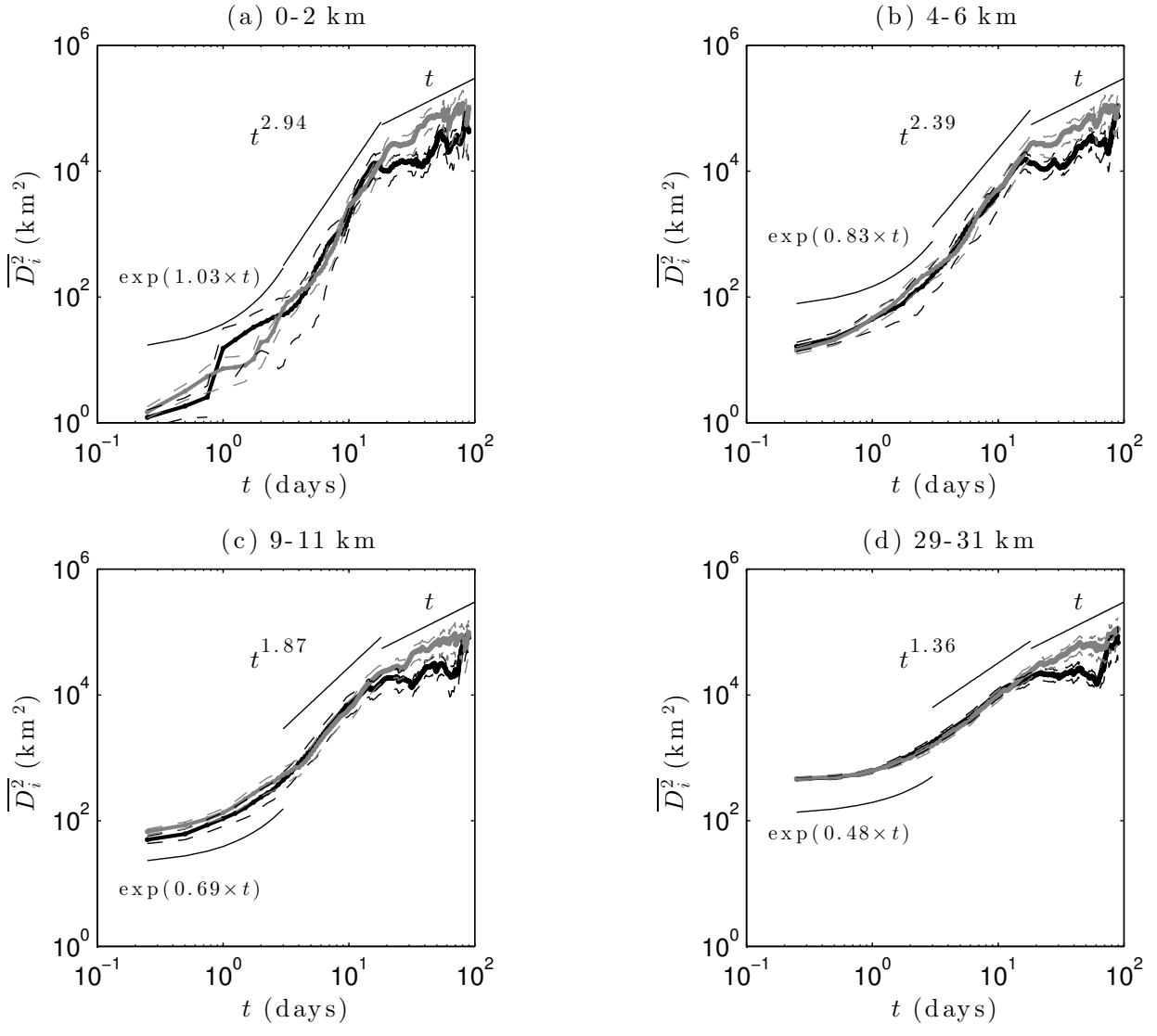

FIG. 3. Relative dispersion vs. time for different ranges of initial separations: (a) 0-2 km. (b) 4-6 km. (c) 9-11 km. (d) 29-31 km. Black (gray) thick curves indicate zonal (meridional) dispersion $\overline{D_1^2}$ ($\overline{D_2^2}$). Dashed lines represent the 90% confidence limits. From 0 to 3 days an exponential curve is fitted; errors of the growth rates are 0.18, 0.09, 0.06 and 0.02 d^{-1}, respectively. From 3 to 18 days the best fit of a power-law in time is shown; errors of the exponents are 0.19, 0.12, 0.09 and 0.05, respectively. From 20 to 100 days a linear curve is drawn.

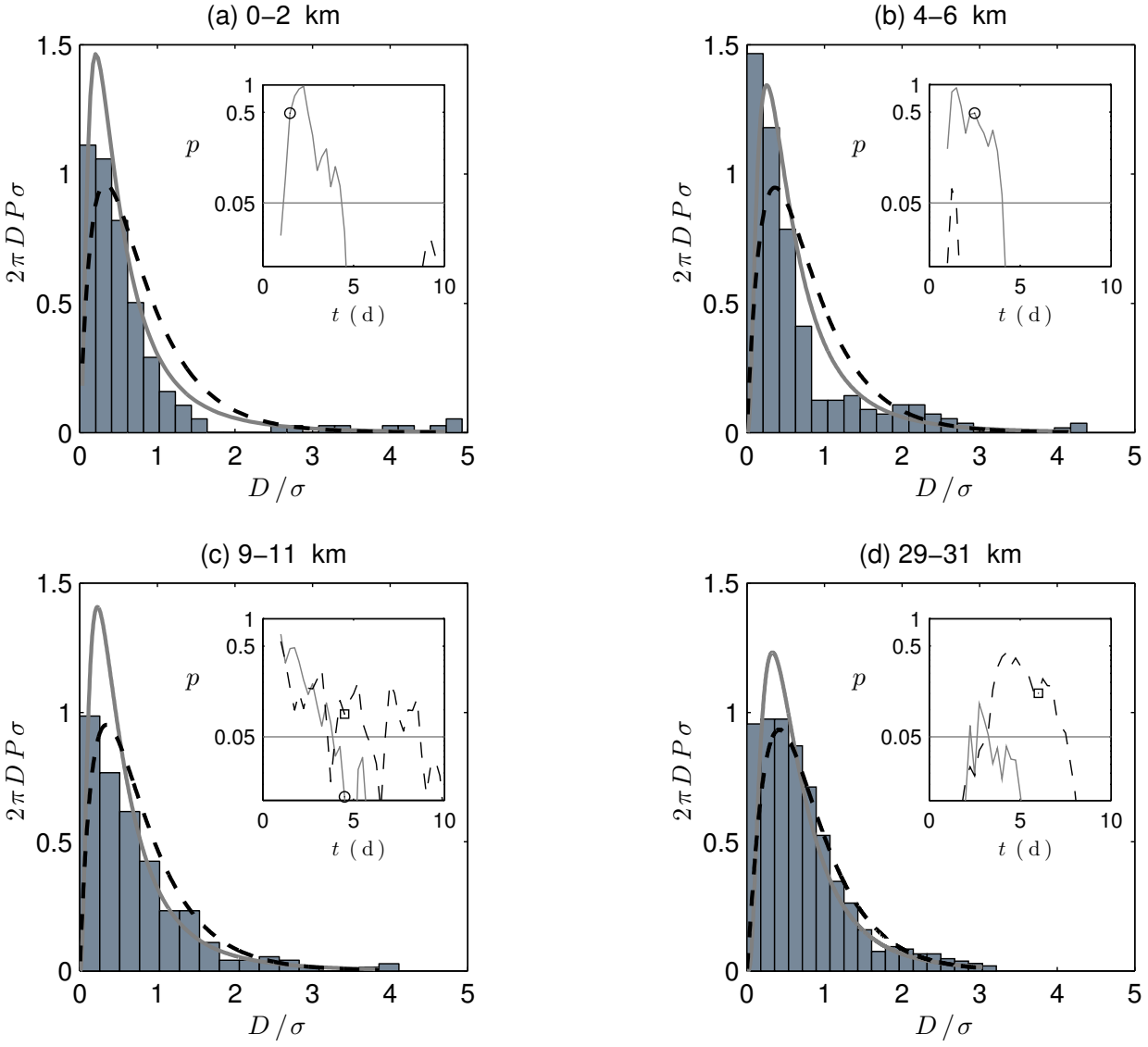

FIG. 4. PDFs of relative separations for the same cases presented in Fig. 3 (panels a to d). Bars indicate PDF values from data at fixed times t_a, re-scaled with the standard deviation of separations σ at that time: (a) $t_a = 1.5$ d, $\sigma = 6$ km; (b) $t_a = 2.5$ d, $\sigma = 19$ km; (c) $t_a = 4.5$ d, $\sigma = 44$ km; (d) $t_a = 6$ d, $\sigma = 91$ km. The curves represent PDFs for the exponential (gray line) and the Richardson (dashed line) regimes, given by expressions (A3) and (A7). The free parameters T (exponential) and β (Richardson) in these examples are $T = [3.7, 8.1, 12.4, 26.1] \pm 1$ d, and $\beta = [0.8, 0.9, 0.9, 0.9] \pm 0.02$ km$^{2/3}$ d^{-1}. The insets show a semi-log scale of the Kolmogorov-Smirnov probability p at different times, with 0.05 significance level (horizontal line). The KS test between the empirical and the exponential (Richardson) distributions is indicated with a solid (dashed) line. The distributions are similar when $p > 0.05$. Circles (squares) indicate the KS test result in the examples.

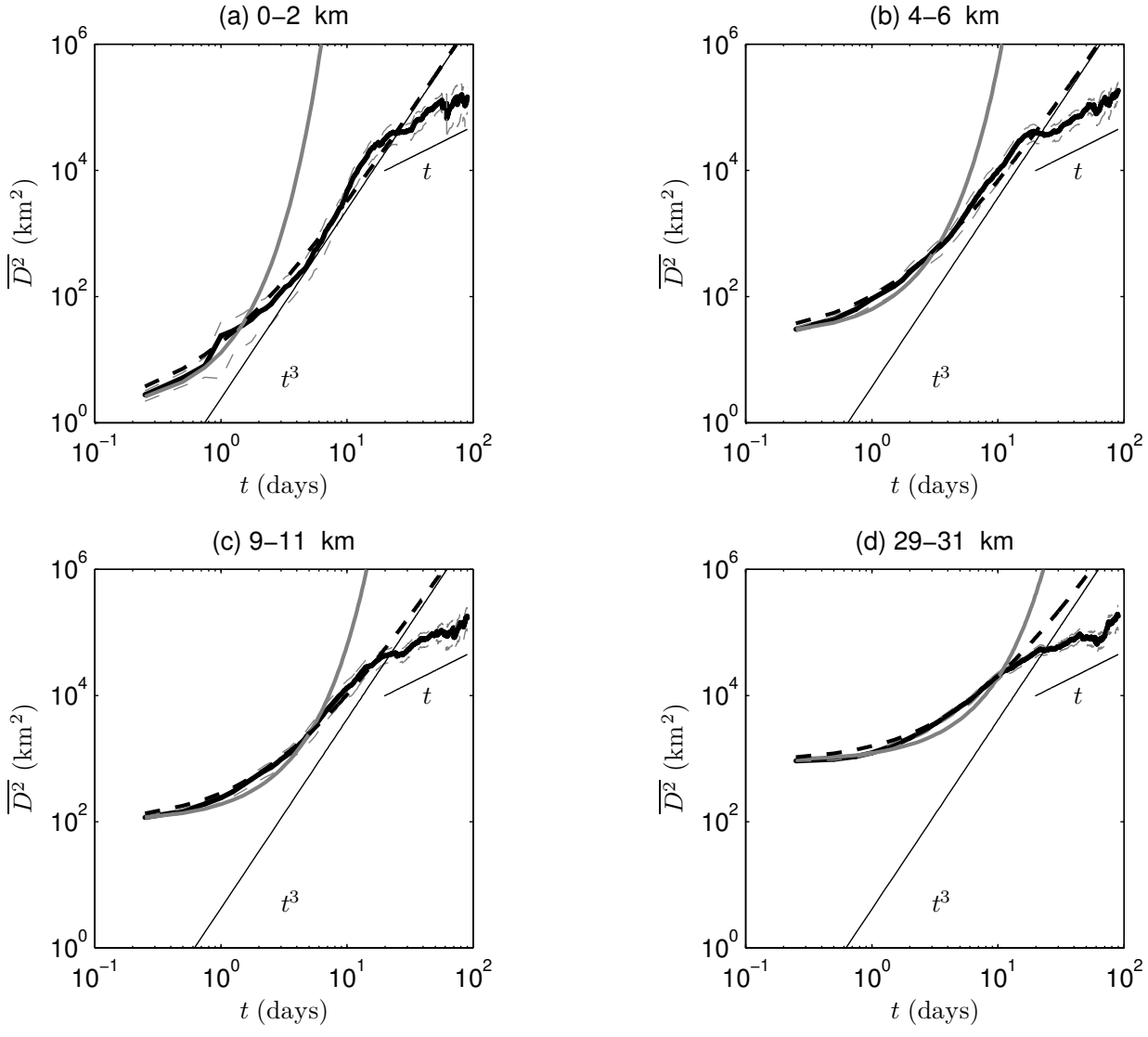

FIG. 5. Relative dispersion vs. time. Thick black curves indicate relative dispersion obtained from data. Gray dashed lines represent the 90% confidence limits. Solid-gray and dashed-black lines denote the exponential and Richardson theoretical regimes, respectively, given by expressions (A4) and (A8) calculated with the corresponding T and β-values shown in Fig. 4. Straight black lines correspond to the asymptotic regimes t^3 (Richardson) and t (standard dispersion for long times).

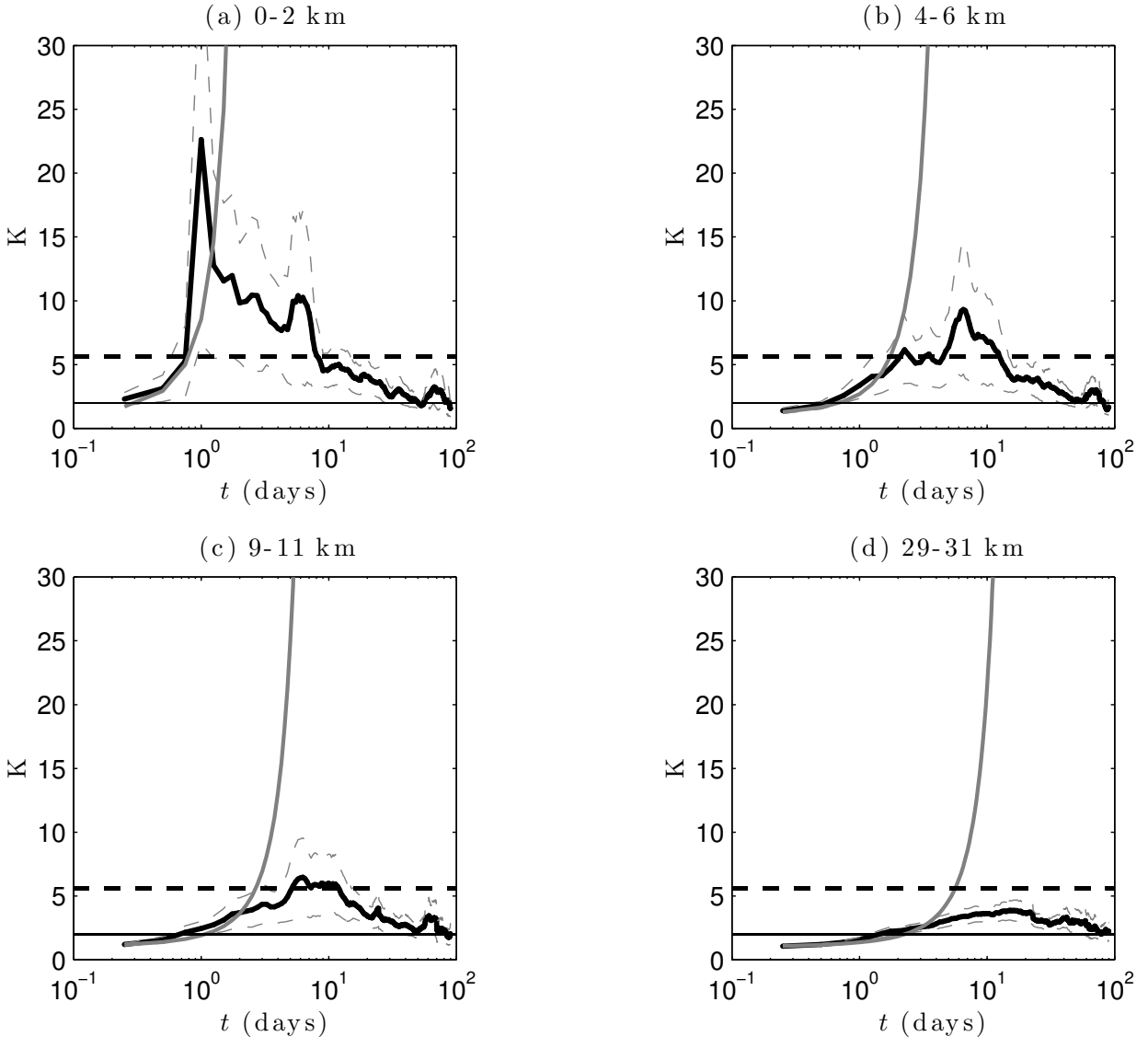

FIG. 6. Kurtosis vs. time. Thick black curves indicate the kurtosis obtained from data. Gray dashed lines represent the error intervals obtained by bootstrapping with 1000 samples. The solid gray line denotes the exponential theoretical curve (A5) calculated with the corresponding T-values shown in Fig. 4. The horizontal lines indicate the asymptotic values of the Richardson regime (dashed line at $K = 5.6$) and standard dispersion (solid line at $K = 2$), respectively.

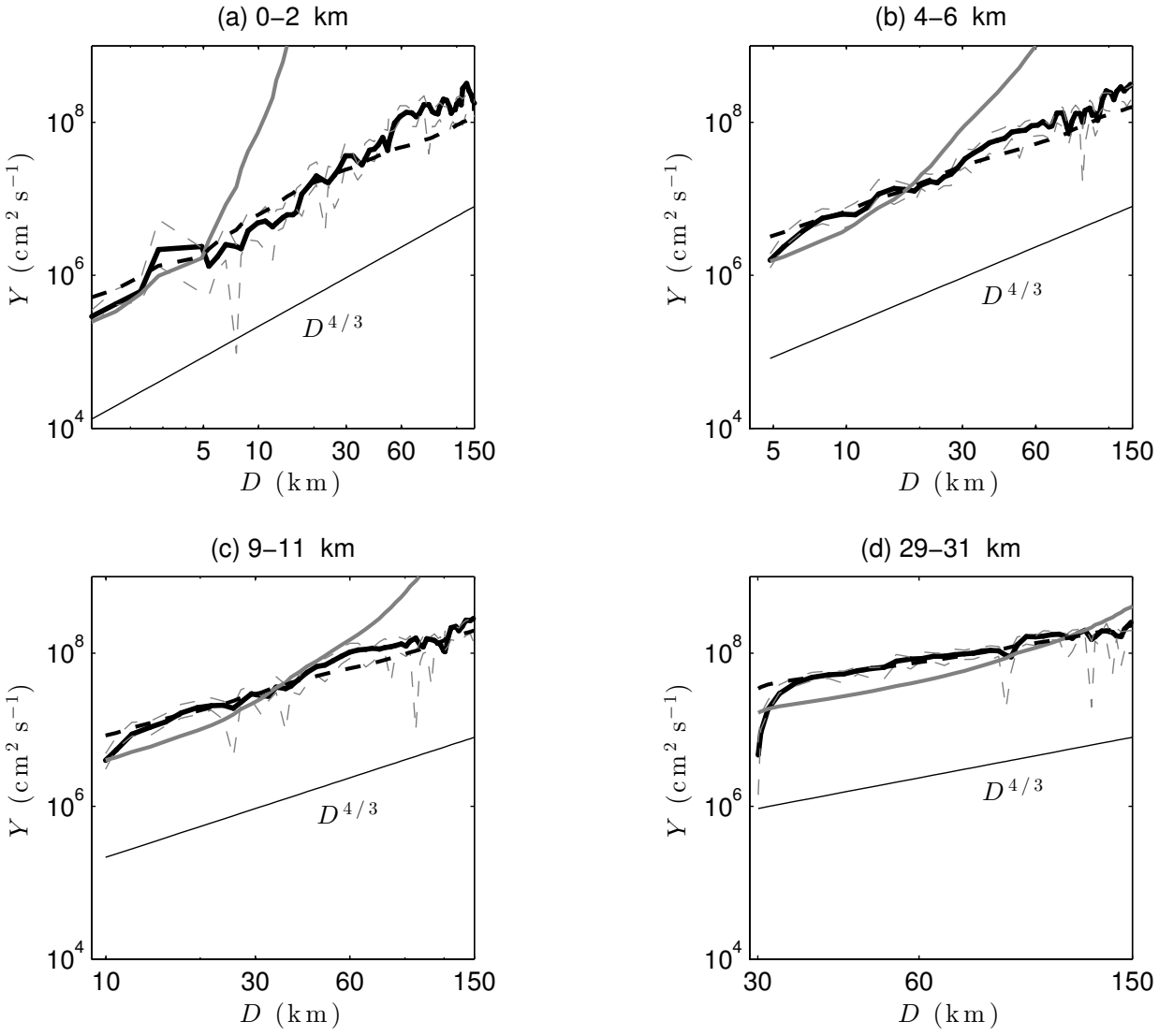

FIG. 7. Diffusivity vs. separation. Thick black curves indicate diffusivity obtained from data by taking (half) the time derivative of the relative dispersion. Gray dashed lines represent the error intervals obtained by bootstrapping with 1000 samples. Solid-gray and dashed-black lines denote the exponential and Richardson theoretical diffusivity curves (A2) and (A6), respectively. The 4/3 Richardson's law is denoted with a straight line.

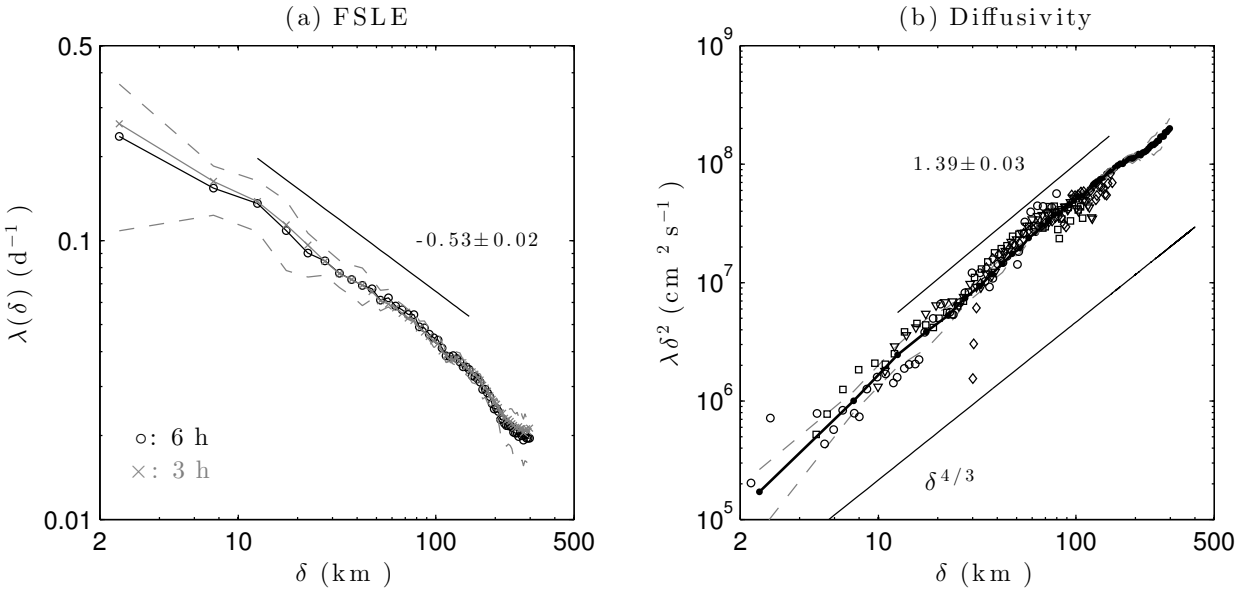

692 FIG. 8. (a) Finite-Scale Lyapunov Exponents (FSLEs) vs. separations for 6 h (black circles) and 3 h (gray
693 crosses) temporal resolution of drifter data. Dashed lines represent the 90% confidence limits of the 6 h resolu-
694 tion data. The bin size is 5 km, the first one centered at 2.5 km. The straight line is the best fit of a power-law
695 between 12.5 and 147.5 km for the 6 h resolution. Numbers are the power-law exponent and the least square
696 error. (b) Diffusivity scale based on the FSLEs for the 6 h temporal resolution (thick line). The upper solid
697 line is the best fit of a power-law in the same range. Symbols indicate relative diffusivities shown in Figure 7
698 (multiplied by 1/3): 0-2 km (circles), 4-6 km (squares), 9-11 km (triangles), 29-31 km (diamonds).

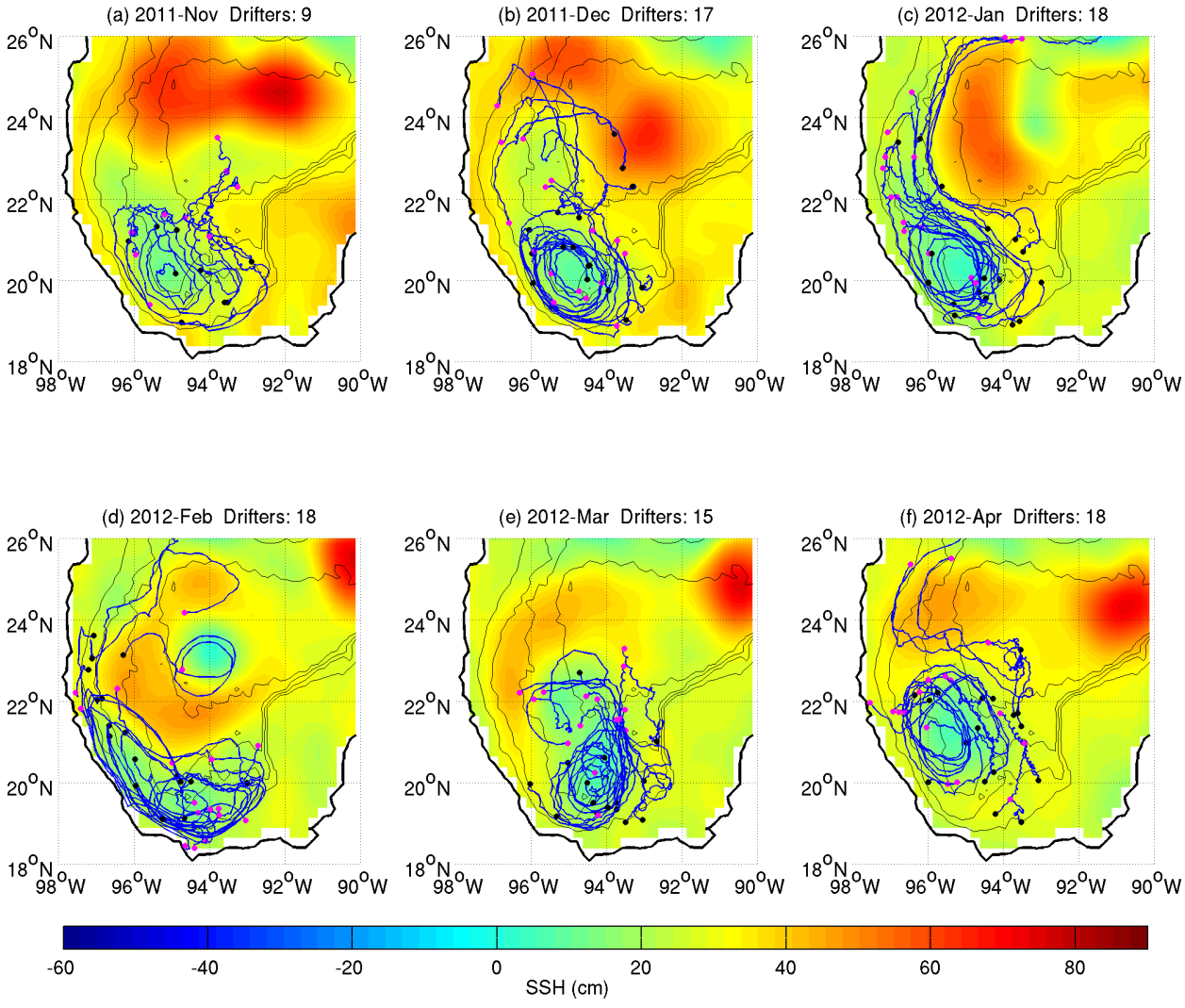

699 FIG. 9. Sequence of six months (November 2011 to April 2012, panels a to f) showing the alternate occurrence
700 of the northward advection and blocking scenarios (see text). Trajectories during the corresponding month are
701 colored in blue. Black (magenta) dots indicate the beginning (end) of the trajectories. The altimetry surfaces
702 correspond to day 15 in each month. Topography contours (500, 1500, 2500 and 3500 m) are denoted with thin
703 black lines.

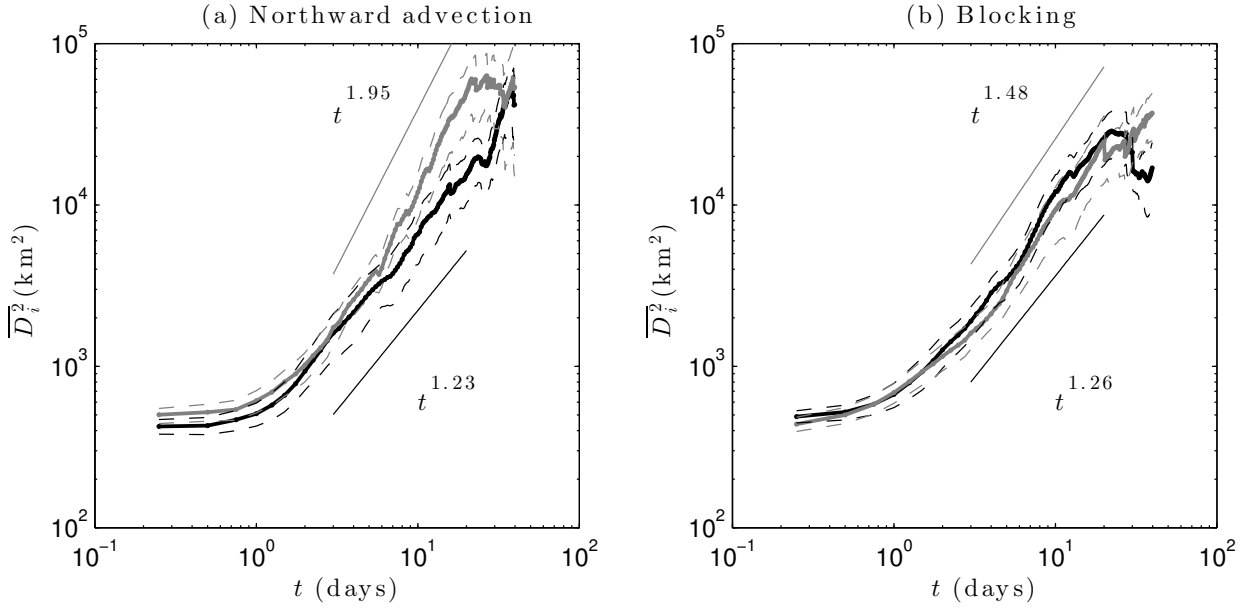

FIG. 10. Relative dispersion vs. time for the dispersion scenarios. (a) Northward advection. The black (gray) curve indicates zonal (meridional) dispersion. Initial separations are in the range of 29-31 km. Dashed lines represent the 90% confidence limits. From day 3 to day 20 a power-law in time is fitted. The error of the exponents are 0.04 and 0.05 for the zonal and meridional components, respectively. The number of pairs at $t = 0$ d is 146, and at $t = 40$ d is 28. (b) Blocking scenario. Curves as in previous panel. The error of the exponents are 0.05 and 0.04 for the zonal and meridional components, respectively. The number of pairs at $t = 0$ d is 145, and at $t = 40$ d is 66.

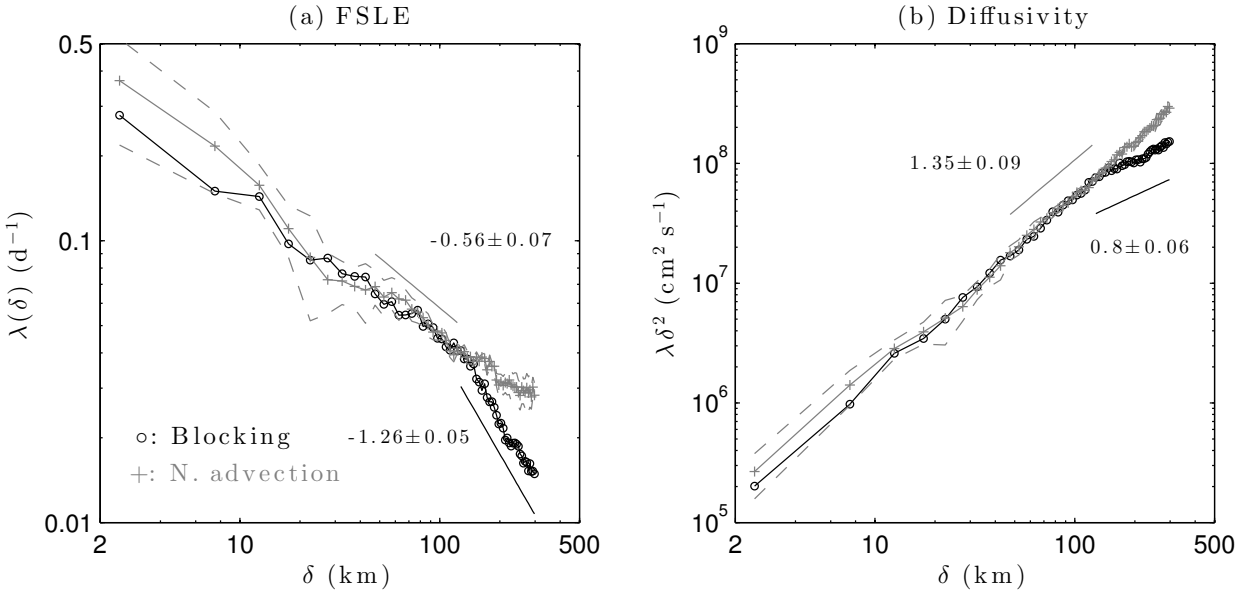

FIG. 11. (a) Finite-Scale Lyapunov Exponents (FSLEs) vs. separations for the dispersion scenarios: northward advection (gray crosses) and blocking (black circles). Dashed lines represent the 90% confidence limits of the northward advection data. The gray (black) solid line is the best fit of a power-law between [47. 5 122.5] km ([127.5 297.5] km) of the northward advection (blocking) data. The numbers indicate the power-law exponents and the least square errors. (b) Diffusivity scale based on the FSLEs. Lines and symbols as in panel a.